



Attenuation of lateral propagating light in sea ice measured with an artificial lamp in winter Arctic

J.-P. Zhao ^{a,*}, T. Li ^{a,1}, D. Barber ^{b,2}, J.-P. Ren ^{c,3}, M. Pucko ^{b,4}, S.-J. Li ^{a,1}, X. Li ^{a,1}

^a Key Lab of Physical Oceanography, Ocean University of China, 238 Songling Road, Qingdao 266100, China

^b Centre for Earth Observation Science, University of Manitoba, Winnipeg, Manitoba, Canada R3T 2N2

^c Institute of Oceanology, Chinese Academy of Sciences, 7 Nanhai Road, Qingdao 266071, China

ARTICLE INFO

Article history:

Received 10 August 2009

Accepted 31 December 2009

Keywords:

Lateral propagating light
Optical attenuation coefficient
Artificial lamp
Arctic
Sea ice

ABSTRACT

The attenuation property of a lateral propagating light (LPL) in sea ice was measured using an artificial lamp in the Canadian Arctic during the 2007/2008 winter. A measurement method is proposed and applied whereby a recording instrument is buried in the sea ice and an artificial lamp is moved across the instrument. The apparent attenuation coefficient $\mu(\lambda)$ for the lateral propagating light is obtained from the measured logarithmic relative variation rate. With the exception of blue and red lights, the attenuation coefficient changed little with wavelength, but changed considerably with depth. The vertical decrease of the attenuation coefficient was found to be correlated with salinity: the greater the salinity, the greater the attenuation coefficient. A clear linear relation of salinity and the lateral attenuation coefficient with $R^2 = 0.939$ exists to address the close correlation of the attenuation of LPL with the scattering from the brine. The observed attenuation coefficient of LPL is much larger than that of the vertical propagation light, which we speculate to be caused by scattering. Part of this scattered component is transmitted out of the sea ice from the upper and lower surfaces.

© 2010 Elsevier B.V. All rights reserved.

1. Introduction

In recent years the extent, thickness and concentration of sea ice in the Arctic Ocean have decreased sharply (Parkinson et al., 1999; Tucker et al., 2001; Lindsay and Zhang, 2005) affecting the Arctic and amplifying global temperature increases (Holland et al., 2006). The perennial sea ice cover dramatically decreased in 2007, continuing a trend that has resulted in a reduction in the September sea ice extent minimum of about 70,000 km²/year over the past 30 years. At this rate we can expect a seasonally ice free Arctic sometime between 2015 and 2030 (Barber and Massom, 2007). With the reduction of the perennial ice we are seeing an increase in the spatial extent and seasonal periodicity of first-year ice. In particular the area of young new ice has increased significantly (Maslanik et al., 2007). Changes in both thickness and extent of young sea ice significantly affect radiative transfer, heat budget of the ocean and, in turn, the timing of ice formation relative to solar insolation in the Arctic.

The apparent optical properties of young ice include diffuse attenuation, albedo and transmission. The apparent optical properties are affected by the light field and the thermophysical characteristics of the sea ice (e.g., brine volume, crystal size, air inclusion, density, etc) through the control which these variables have on the inherent optical properties of young sea ice (e.g., absorption coefficient, scattering coefficient and phase function). The scattering of solar radiation is controlled by the volume fractions of brine, ice and air, their relative number densities, and the geometry of particular scattering inclusions (Schoonmaker et al., 1989). Laboratory experiments primarily focus on two measurements: the scattering phase function reveals the scattering flux in different directions (Gilbert and Schoonmaker, 1990; Voss and Schoonmaker, 1992; Voss et al., 1992) and the scattering coefficient, which determines the attenuation of radiative fluxes through the sea ice. The scattering coefficient of sea ice varies from 10 m⁻¹ in warmer sea ice to about 200 m⁻¹ in cold ice or bubble rich ice (e.g., Perovich and Grenfell, 1981).

As a natural phenomenon, scattering in sea ice can also be measured *in situ* (e.g., Haines et al., 1997) relying upon *in situ* measurement of thermophysical properties and direct measurement of particular apparent optical properties parameters. Laboratory experiments use a narrow collimated light beam whereas *in situ* solar radiation has an infinite width which affects how the light scatters. Field measurements to-date have been concentrated on vertically propagating lights (Perovich et al., 1998) where forward propagating light relates to the transmission and energy flux of light through sea ice, and backward propagating light is concerned with the crucial role surface albedo plays in the surface energy balance and remote sensing. Observations of

* Corresponding author. Tel./fax: +86 532 66782096.

E-mail addresses: jpzhaou@ouc.edu.cn (J.-P. Zhao), litaoocean@ouc.edu.cn (T. Li), dbarber@ms.umanitoba.ca (D. Barber), jpren@ms.qdio.ac.cn (J.-P. Ren), mpucko@emcpl.eu (M. Pucko), lisj@ouc.edu.cn (S.-J. Li), lixiangouc@ouc.edu.cn (X. Li).

¹ Fax: +86 532 66782096.

² Present address: University of Manitoba, Winnipeg, Manitoba, Canada R3T 2N2. Fax: +1 204 272 1532.

³ Present address: Chinese Academy of Sciences, 7 Nanhai Road, Qingdao 266071, China. Fax: +86 532 82898519.

⁴ Fax: +1 204 272 1532.

directional propagating light in natural sea ice volumes are rare in the literature (e.g., Maffione et al., 1998; Pegau and Zaneveld, 2000).

The solar energy that entered into the sea ice is attenuated not only in the vertical direction, but also by its lateral propagation. The attenuation of the laterally propagating light (LPL) of the incident radiation is an important pathway to consume the solar energy. The attenuation of light in sea ice is anisotropic; perpendicular to the air–ice interface. It is depth-dependent (Perovich, 1996) and horizontally the attenuation is different from that in the vertical (Haines et al., 1997; Trodahl et al., 1989). Our motivation was to characterize the attenuation of LPL, to improve our understanding in thermodynamics of sea ice, which may assist in radiative transfer modeling. Buckley and Trodahl (1987a,b), Trodahl et al. (1987) and Haines et al. (1997) presented their experiments on the Antarctic sea ice by a novel measuring geometry and a quartz-halogen lamp to measure the anisotropic scattering of light, the scattering length, their correlation with salinity, and the different optical properties in the surface, bulk and algae layers. A similar but modified measuring geometry was adopted in this study to design a field experiment using a flat artificial lamp and putting the instrument into the ice to measure the LPL on winter sea ice. The purpose of the experiment is to see if LPL measurements add to our understanding of how light is attenuated parallel to the air–ice interface by sea ice physical properties (ice grains, brine channels and air bubbles) and how this may be related to thermodynamic changes in young sea ice. Ultimately we may be able

to invert the characteristics of LPL to infer geophysical characteristics of the ice without disturbing the ice sample through manual extraction and micro-structural analysis. We first attempt to correlate the attenuation of LPL with sea ice salinity.

One of the problems of investigating young sea ice is that the *in situ* measurements are difficult due to the high temperature of the sea ice (e.g., Ehn et al., 2007). When young ice cores are removed, brine tends to drain, and the relative proportions of ice, brine and air in samples transferred to a cold lab change due to the lower temperature of the cold lab (Ehn et al., 2007). Inclusion geometry may also change when the ice is taken from its native environment resulting in significant changes in the scattering and absorption of light (e.g., Light et al., 2003). In this paper we investigate the utility of an artificial light source to estimate the lateral propagation of spectral radiation as a means of estimating the physical properties of the surface and/or volume of young sea ice.

2. Methods

A team of international investigators participated in the International Polar Year (IPY) Circumpolar Flaw Lead (CFL) system study between November 8th, 2007 and January 31st, 2008, aboard the Canadian Research Icebreaker *Amundsen* in the Southern Beaufort Sea (Fig. 1). A series of sampling stations were selected based upon the overarching sampling plan of the CFL project. Each site was located within the CFL study region where a wide range of sea ice types could be sampled. An

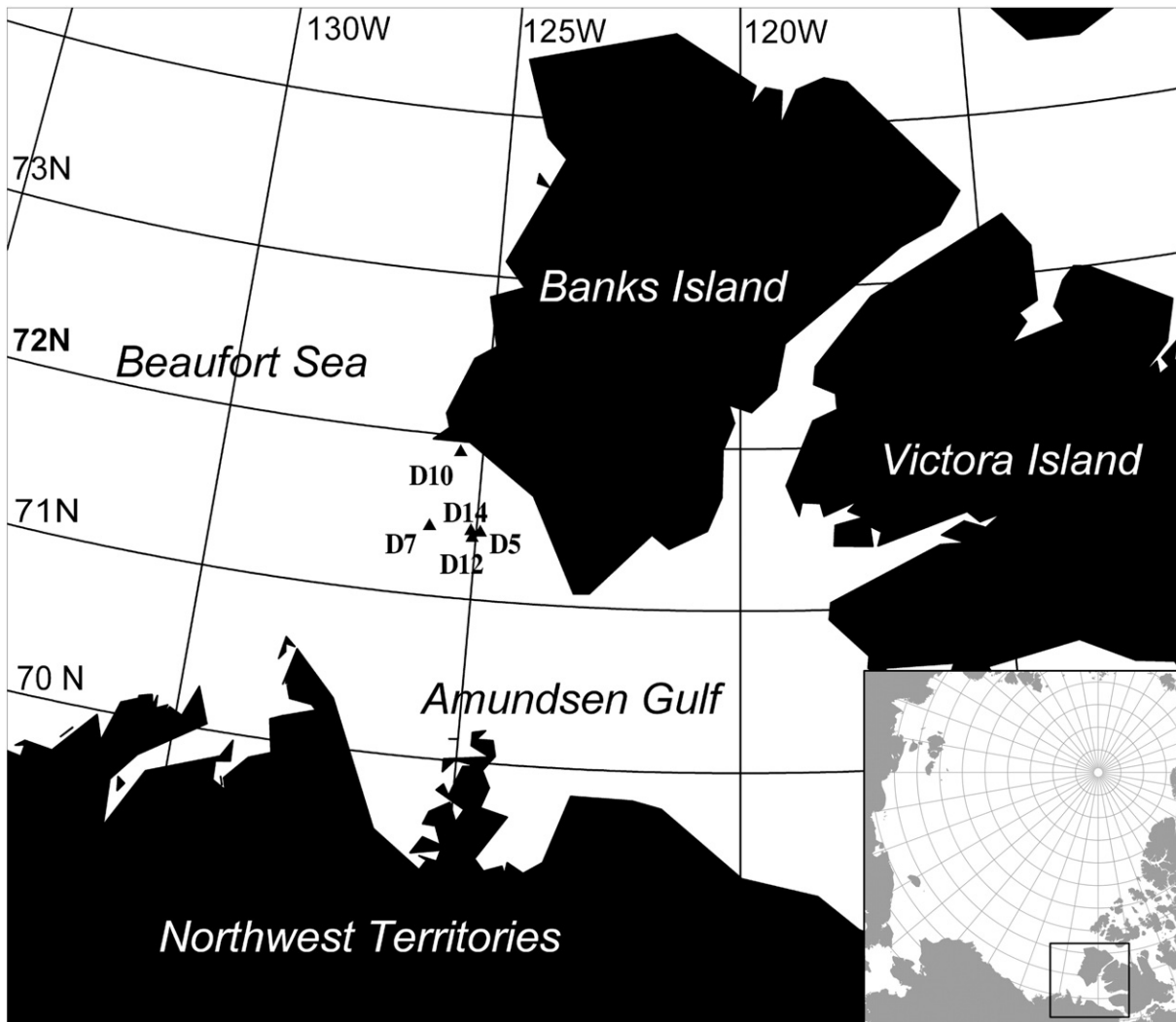


Fig. 1. Experimental stations for lateral propagating light measurements in the Amundsen Gulf. The black square in the insert map on the lower right corner is the location of the observed region in the Arctic.

artificial light source was used to measure the attenuation of LPL in naturally occurring sea ice at these sampling stations. In Fig. 1, Station D10 was located in fast ice while the others were on mobile pack ice. Stations D5, D12 and D14, although close together on the figure, were separate drifting ice floes. During our experiment, all the sea ice was first-year ice with a thickness of between 0.5 and 1.2 meters (m). To standardize for surface illumination all LPL measurements had to be conducted in darkness.

2.1. The lamp

A custom-designed artificial lamp consisting of ten fluorescent bulbs and measuring 1.3 m by 0.96 m was constructed for ease of transport and use on the sea ice. The artificial light contains all the wavelengths of naturally occurring solar radiation within 313–870 nm, though the spectral distribution of the lamp is different from the solar radiation (Zhao et al., 2008). As the experiment was concerned with the attenuation rate rather than irradiance, the lamp was suitable for attenuation rate measurements. The backboard and frame of the lamp were painted white and a crystal plastic board covered the bulbs to increase the uniformity of the light. The lamp's performance was tested under indoor and outdoor conditions by the same instrument PRR-810 including the uniformity and stability of the irradiance produced, the divergence of the light beam, the marginal effect of the lamp and the impacts from changes in temperature. As estimated by Zhao et al. (2008), the maximum relative error of the measured irradiance brought by the lamp was less than 3%, which is the accuracy of the light source and is considered satisfactory for the experiment. This error does not include the “measuring error”, which needed to be controlled during each measurement.

2.2. Instrument and fore-optics

The surface unit of the Profiling Reflectance and Radiometer System (PRR-810) from Biospherical Inc. (USA) was used to measure LPL. The PRR-810 is equipped with eighteen (18) wavebands from 313 nanometers (nm) to 870 nm with the bandwidth of 10 nm and includes a cosine collector appropriate for hemispheric field-of-view observations. In order to accurately measure the attenuation of the LPL, a method to reduce the field-of-view of the instrument was necessary to collect light only from a very small solid angle of the horizontal. A fore-optic with a diameter of 0.01 m and a length of 0.1 m was attached to the PRR-810 to produce an half field-of-view of 2.9° (8.5° if the cosine collector of 0.02 cm is considered) as adopted by Hanesiak et al. (2001).

2.3. Observations

As the consistency of the relative movement, the lamp movement measurement is equivalent to the measurement using a fixed lamp and a moving instrument. The PRR-810 was placed in a fixed position while the lamp was moveable (Fig. 2) after the snow cover was

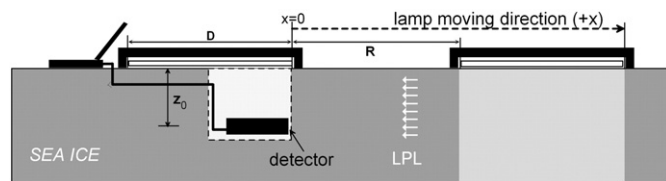


Fig. 2. Sketch of the experiment for the attenuation of lateral propagating light where a trench is cut and an optical instrument is buried with the face of the detector to the right. The start position of the right edge of the lamp is at $x = 0$, and it is moved to the right, $+x$ direction. The lateral propagating light (LPL) is transferred from the shining region to the left and reaches the detector. D is the width of the lamp. The length of the lamp is demanded to be sufficiently large exceeding the field-of-view of the instrument. R is the value of the left edge of the lamp at the x -coordinate, which is negative if the left edge of the lamp moves at the left of the detector. Data are obtained in real time with a computer.

cleaned off the ice. A trench was cut in the sea ice using an auger, and the detector side was flattened and polished to remove any matter that could affect scattering and to minimize the reflection of the light from the interface. The PRR-810 was then positioned in the trench horizontally. The detector of the PRR-810 was placed as close as possible to the ice with little space, and a black cloth was used to prevent ice falling into the space during refilling of the trench. The instrument was buried and the top surface of the trench was smoothed out to facilitate the movement of the lamp on the surface (Fig. 2). If the trench is dug too deep, seawater may percolate into the trench through the underlying sea ice. Measurements began with the detector in the bottom of the trench nearest the ice–water interface, and progressed upward in the trench by filling up the trench with snow and to the next measurement level and replacing the detector. The lamp was moved step by step by a marked rope and a wooden stick. The lower end of the stick was an axis fixed on the ground and the stick was swung around the lower end to let the rope move 5 cm each swing. The lamp was positioned facing downwards with shorter side (0.96 m) parallel to the direction of movement and the longer side (1.3 m) perpendicular to the direction of movement. The irradiance from the lateral propagating light was measured by the radiometer (Fig. 2). The lamp's starting position was with the centre of the lamp aligned with the axis of the PRR-810 and with the margin of the lamp aligned with the PRR-810's front face. The lamp was then moved in increments of 0.05 m at intervals of 1–2 s until the lamp was beyond the range of the PRR-810. The radiometer data were collected in real time and were monitored via a computer. Note that all measurements were made at night in darkness. On days where the moon was visible we covered the measurement site with a black cloth.

3. Relative variation of irradiance of LPL with distance from the lamp

Since the field-of-view of the PRR-810 fore-optic was quite small, we speculate that the observed irradiance was dominated by the scattering light parallel to the axis of the PRR-810. The origin of the z -coordinate was the upper surface of the sea ice, the depth of the PRR-810 was at z_0 from the surface, and the x -axis was the horizontal distance between the right margin of the lamp and PRR-810 (Fig. 2). When the lamp was moved to the front of the PRR-810 ($+x$ direction), the variation in irradiance with distance was as shown in Fig. 3.

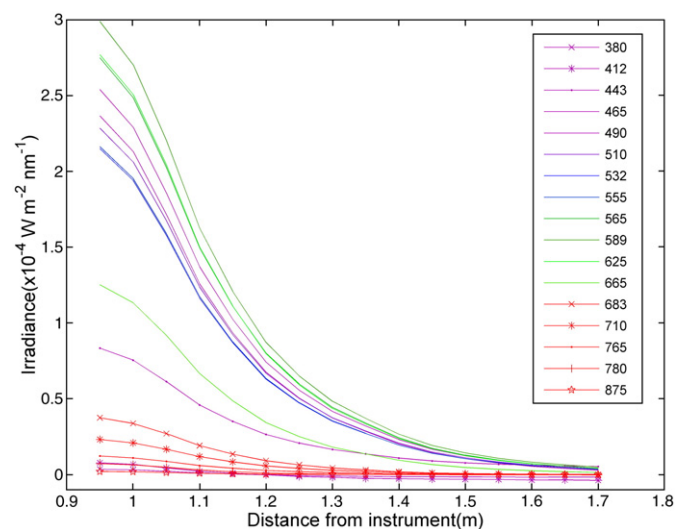


Fig. 3. Irradiance varied with the distance when the lamp was moved at Station D5. The distance of the lines is plotted from $x = 0.96$ when the left margin (Fig. 2) of the lamp leaves the vertical plane the instrument located.

Records for seventeen (17) of the wavelengths were of acceptable quality, with the exception of the 313 nm wavelength which was of low intensity in the light source resulting in a weak signal. The irradiance was found to increase as the lamp moved to its closest position over the PRR-810 where it reached its maximum. Irradiance then decreased rapidly as the lamp moved away as shown in Fig. 3.

As movement of the lamp altered the illumination conditions, the resulting curves (Fig. 3) reflect the transmission of lateral propagating light as a function of distance. By dividing the irradiance of each record by the irradiance $E'_{ref}(z, \lambda, x_0)$ at an arbitrary point as a reference value, the relative variation of irradiance was obtained.

$$E'(z, \lambda, x) / E'_{ref}(z, \lambda, x_0) \quad (1)$$

To reduce the error of the relative variation, usually the maximum irradiance is chosen as the reference value. Taking the logarithmic relative variation of irradiance (hereafter referred to as “logarithmic relative variation rate”) as the vertical coordinate, the same data used in Fig. 3 are shown in Fig. 4.

When all of the lamp were moved to the front and then beyond the PRR-810, as shown on Fig. 4 where the lamp movement distance exceeds 0.96 m, the logarithmic relative variation rate illustrated a strong linear extinction, hereafter referred to as the ‘linear portion’ of the relationship (Fig. 4). The formula appropriate for this ‘linear portion’ is

$$\mu(\lambda)(x-x_0) = -\ln \left[\frac{E'(z, \lambda)}{E'_{ref}(z, \lambda)} \right] \quad (2)$$

The slope of the straight line is the attenuation coefficient of LPL, $\mu(\lambda)$, which explains the physical significance of the linear portion in Fig. 4. The seven curves with the larger slopes, plotted in red and violet respectively, represent the red, infrared and near violet wavebands, which demonstrate stronger attenuation of the light at these wavelengths. The attenuation coefficients for the remaining nine wavebands (465–665 nm) are quite similar with nearly the same magnitudes. Light of 443 nm is obviously special with less linearity and less attenuation than the others. For polycrystalline pure ice,

absorption is dominant and the attenuation is stronger in red and infrared wavelengths (Grenfell and Perovich, 1981). Here, attenuation at 380 nm and 412 nm is greater than attenuation at 875 nm, which can be explained by the scattering generated by significant quantities of some impurity in the ice.

4. Attenuation coefficient of lateral propagating light and its vertical distribution

The attenuation coefficient of LPL, $\mu(\lambda)$, is calculated by the best-fit of the linear portion of the relative variation rate curve in Fig. 4. The spectral distribution of the attenuation coefficient of LPL at each level for Station D7 is displayed in Fig. 5. It shows that the spectral distributions at different levels are quite similar, but decrease with depth. The attenuation coefficients for wavelengths greater than 700 nm are much greater, because the light is more strongly absorbed by the sea ice in these wavelengths. With the exception of the red frequencies, the attenuation coefficients from 465 nm to 665 nm in each level are nearly equal to a constant. This is an interesting result, as it is quite different from the spectral attenuation of direct incident light, which is wavelength-dependent (Maykut and Grenfell, 1975). The outstanding difference might be because of the dominating light. In the vertical direction, the transmitted light is mainly influenced by selective absorption by foreign material within the ice to produce the spectrum-dependent attenuation (Maykut and Grenfell, 1975). Whereas, the lateral propagating light is mainly scattering light, whose attenuation could be assumed to be a constant with wavelength (Grenfell, 1983, 1991).

The attenuation coefficients at different levels at Stations D5, D7, D10, and D12 are listed in Table 1, and show an obvious downward trend for all wavelengths. As an example, attenuation coefficients at 490 nm at each level are plotted in Fig. 6. At all the stations, the attenuation coefficients decrease with depth. At Station D7 (ice thickness = 0.77 m) and D14 (ice thickness > 1 m), attenuation is quasi-linear and decreasing with depth, whereas at Station D10, the attenuation coefficients are linear and abruptly decrease above the depth of 0.4 m, and a weaker decrease below that depth.

Although the attenuation coefficients at the same level at different sites are obviously different, the slopes of the attenuation coefficient's vertical variation are similar. Usually the vertical attenuation of solar radiation is caused by brine and air bubbles in the sea ice (Maykut and Light, 1995). In our study, the ice cores were cut into 2.5 cm thick layers and melted in tightly closed HDPE containers for the salinity

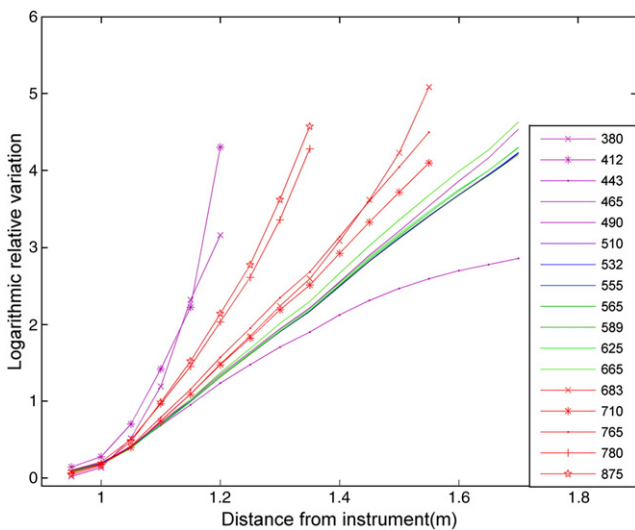


Fig. 4. Logarithmic relative variation of all wavelengths with the movement of the lamp at Station D5. The distance of the lines is plotted from $x = 0.96$ when the left margin (Fig. 2) of the lamp leaves the vertical plane the instrument located. The nine wavelengths from 465 to 665 nm attenuate in a similar rate. The five red lines for red and infrared wavelengths and two violet lines for near violet wavelengths present greater attenuation. Light of 443 nm is obviously special with less linearity and less attenuation than the others.

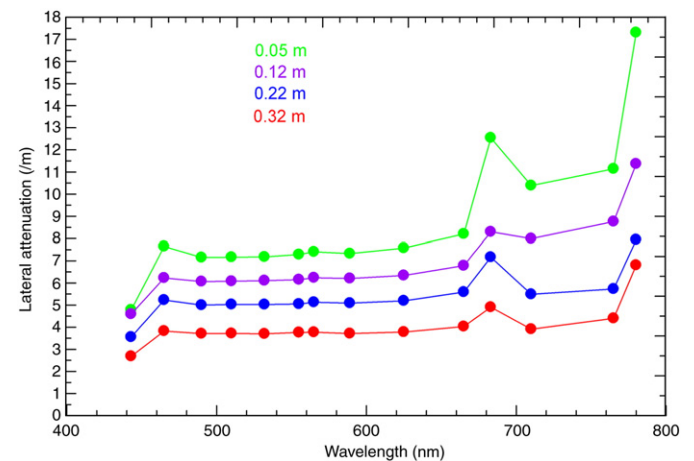


Fig. 5. Spectral distribution of the attenuation coefficients of lateral propagating light in each level at Station D7. The results for 313, 380, 412, and 875 nm are not presented as the attenuation for these wavelengths was much larger.

Table 1
Attenuation coefficient of lateral propagating light, $\mu(\text{m}^{-1})$.

Stations	D5					D7					D10					D12			
	Depth(m)	0.12	0.05	0.12	0.22	0.32	0.10	0.20	0.30	0.40	0.50	0.15	0.25	0.35	0.45				
Wavelength (nm)	443	3.79	4.78	4.59	3.55	2.68	4.25	3.95	3.14	2.13	1.48	4.13	3.39	2.64	2.14				
	465	6.34	7.64	6.22	5.23	3.82	7.71	6.79	4.96	3.53	3.20	7.60	5.56	4.95	4.76				
	490	5.87	7.15	6.06	4.99	3.70	7.37	6.30	4.71	3.39	2.98	7.15	5.30	4.58	4.29				
	510	5.88	7.16	6.08	5.03	3.72	7.42	6.39	4.73	3.38	2.98	7.09	5.30	4.63	4.35				
	532	5.88	7.17	6.10	5.02	3.70	7.48	6.42	4.73	3.38	2.99	7.17	5.34	4.60	4.38				
	555	5.90	7.28	6.15	5.05	3.76	7.60	6.51	4.79	3.40	3.05	7.18	5.41	4.65	4.38				
	565	6.02	7.40	6.23	5.13	3.77	7.75	6.62	4.88	3.48	3.09	7.45	5.54	4.83	4.54				
	589	5.87	7.32	6.20	5.09	3.71	7.57	6.56	4.85	3.45	3.02	7.32	5.45	4.74	4.41				
	625	6.01	7.57	6.34	5.19	3.78	7.94	6.84	5.03	3.57	3.16	7.68	5.68	4.92	4.62				
	665	6.52	8.20	6.78	5.59	4.03	9.02	7.70	5.54	3.96	3.52	8.68	6.42	5.57	5.26				
	683	9.37	12.54	8.29	7.16	4.90	15.30	9.53	7.31	5.17	6.25	13.48	8.34	8.15	5.71				
	710	7.04	10.39	7.97	6.59	4.45	11.47	8.24	6.44	4.37	4.79	10.35	7.10	6.00	6.79				
	765	7.97	11.14	8.40	7.01	4.87	11.37	8.96	6.74	4.39	4.57	10.25	7.50	6.62	6.40				
	780	10.55	19.99	11.55	9.23	8.41	15.94	12.11	7.37	5.07	5.51	15.64	15.96	6.55	6.22				

vertical profile analysis. Salinity of melted sea ice samples was subsequently calculated from conductivity and temperature using HACH SENSION5 portable conductivity meter. The close correlation between the attenuation coefficient and sea ice salinity is addressed in Fig. 7. It is clear that the attenuation coefficient is proportional to the salinity in sea ice. Both reach their maximum in the upper level at Stations D12 and D14. At Station D12 however, the attenuation coefficient below 0.3 m changed only a little due to constant salinity. The LPL attenuation coefficients for green and blue light wavelengths are nearly constant at certain levels, hinting that the attenuation caused by salinity is independent of these wavelengths. The measured results of attenuation coefficient and salinity for all stations are plotted in Fig. 8. A clear linear relation with $R^2=0.939$ exists to address the close correlation of the attenuation of LPL with the scattering from the brine. It is interesting to note that a similar correlation between optical extinction and salinity was found during radiative transfer studies in spring sea ice (Ehn et al., 2008) focusing on natural light and apparent optical properties measurements normal to the surface.

The observed LPL attenuation coefficient is much larger than that of vertically propagating light. For example, the lateral attenuation coefficients at 490 nm are about 3.0–7.5 m^{-1} (Table 1), indicating a

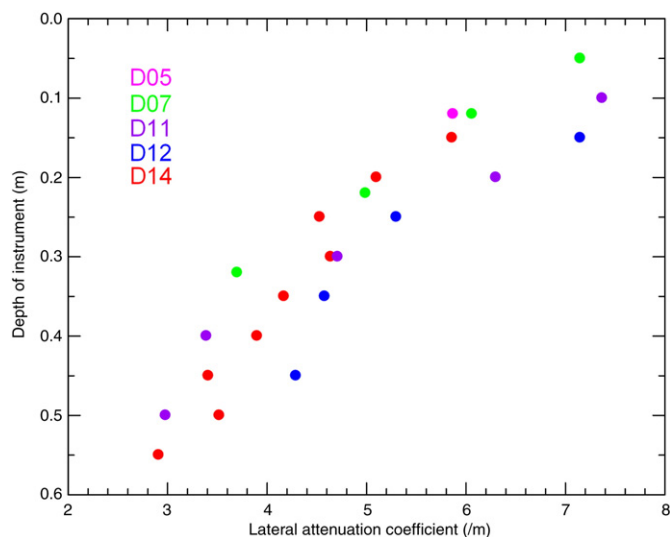


Fig. 6. Vertical variation of the attenuation coefficient of LPL for 490 nm.

strong attenuation for a laterally propagating light. However, the attenuation coefficient for a vertically propagating light at the same wavelength is less than 1.0 m^{-1} (Perovich et al., 1998). This result is quite similar with the experimentally-determined scattering coefficients discussed by Haines et al. (1997), in which the attenuation in the horizontal is 2–3 times larger than in the vertical direction.

Preferential propagation in the vertical dimension is likely due to the columnar structure of the sea ice crystals, as described by Ehn et al. (2007). We postulate that the reason for stronger lateral attenuation is that part of the LPL is scattered vertically, leaking out of the sea ice at its upper and lower surfaces. However, in vertical scattering, part of the vertical propagating light is scattered laterally, but no “leaking” appears as nearly the same amount of scattered light will backscatter from the neighboring ice. Further investigation of this phenomenon is ongoing.

5. Conclusion

In this study, the attenuation of lateral propagating light in sea ice is investigated by an in situ experiment. The main conclusions are as follows:

A measurement method for the attenuation of lateral propagating light (LPL) is proposed and applied in this study by burying a spectral radiometer (PRR-810) in the sea ice and by moving a flat artificial light source within a fixed range parallel to the ice surface. The method is verified to be operational on sea ice in the dark. Because the LPL attenuation coefficient is related to the microstructure of sea ice, the experiment is useful for the investigation of the *in situ* micro-structural properties of sea ice.

The apparent attenuation coefficient $\mu(\lambda)$ is obtained from the ‘linear portion’ of the measured logarithmic relative variation rate. With the exception of blue and red lights, the LPL attenuation coefficient changed little with wavelength, but changed considerably with depth. The vertical decrease of the attenuation coefficient was found to be correlated with salinity: the greater the salinity, the greater the attenuation coefficient. A clear linear relation of salinity and the lateral attenuation coefficient with $R^2=0.939$ exists to address the close correlation of the attenuation of LPL with the scattering from the brine.

The observed attenuation coefficient of LPL is much larger than that of vertical propagation light. The preferential propagation in the vertical dimension is likely due to the columnar structure of the sea ice crystals. The reason for stronger lateral attenuation, we postulate, is that part of the LPL is scattered vertically and leaks out of sea ice from its upper and lower surfaces.

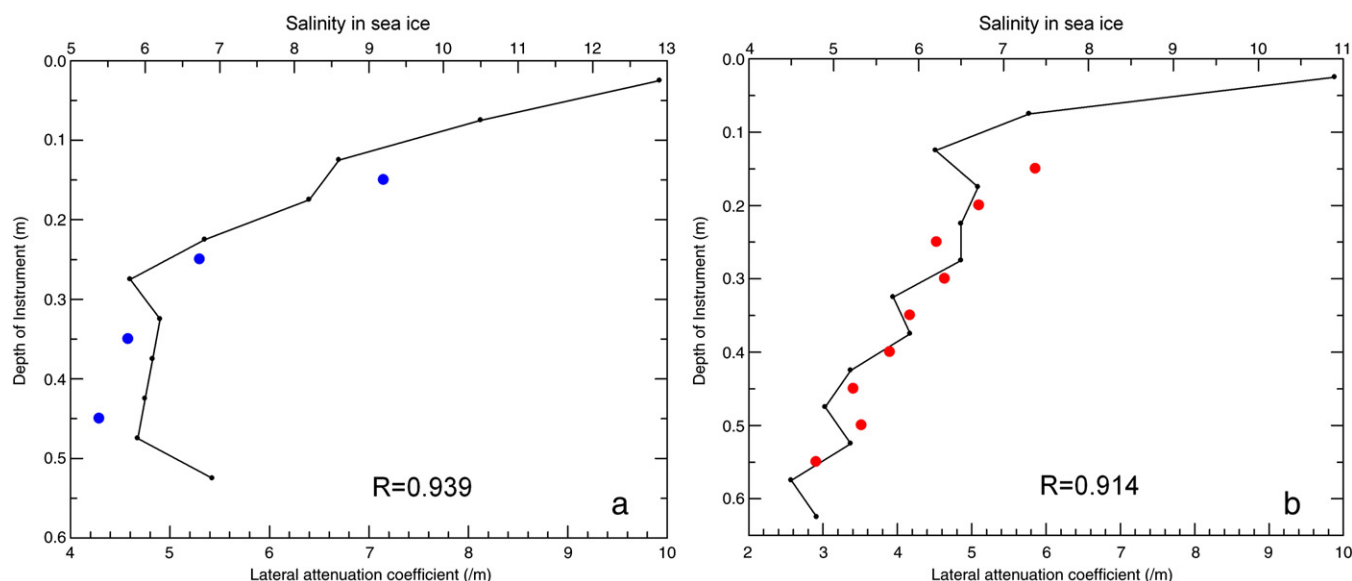


Fig. 7. Correlation of the attenuation coefficient of LPL with salinity in sea ice for the light of 490 nm; (a) Station D12 and (b) Station D14. Dots express the attenuation coefficient of the lateral propagating light, and lines are the salinity (psu) in sea ice. The correlation coefficients for both stations are 0.939 (D12) and 0.914 (D14), respectively.

Acknowledgements

This study was supported by the Nature Science Foundation of China (No. 40631006) and the International Polar Year Program of China. The field experiment was supported by the Canadian International Polar Year program office through a grant to DGB. The Centre for Earth Observation Science, University of Manitoba provided in field and logistical support for this work. We appreciate the assistance of the Circumpolar Flaw Lead System Study Chief Scientists Dr. Gary Stern, Dr. Tim Papakyriakou, and Dr. Jody Deming for their support. We would like to thank the Captains and Crew of the CCGS *Amundsen* for their excellent field support during the cruise. Thanks to Jens Ehn and Ryan Galley (U of M) for the pre-reviews of this manuscript and to T. Maconachie (U of M) for editorial assistance.

References

Barber, D.G., Massom, R.A., 2007. The role of sea ice in Arctic and Antarctic Polynyas. In: Smith, W.O., Barber, D.G. (Eds.), *Polynyas: Windows to the World: Elsevier Oceanography Series*, vol. 74, pp. 1–54.

Buckley, R.G., Trodahl, H.J., 1987a. Scattering and absorption of visible light by sea ice. *Nature* 326, 867–869 doi:10.1038/326867a0.

Buckley, R.G., Trodahl, H.J., 1987b. Thermally driven changes in the optical properties of sea ice. *Cold Regions Science and Technology* 14, 201–204.

Ehn, J., Hwang, B.J., Galley, R., Barber, D.G., 2007. Investigations of newly formed sea ice in the Cape Bathurst polynya: Part 1. Structural, physical and optical properties. *Journal of Geophysical Research* 112 (C05002).

Ehn, J.K., Mundy, C.J., Barber, D.G., 2008. Bio-optical and structural properties inferred from irradiance measurements within the bottommost layers in an Arctic landfast sea ice cover. *Journal of Geophysical Research* 113 (C03S03).

Gilbert, G.D., Schoonmaker, J., 1990. Measurements of beam spread in new ice. *Proceedings of SPIE Ocean Optics VIII*, vol. 1302, pp. 545–555.

Grenfell, T.C., 1983. A theoretical model of the optical properties of sea ice in the visible and near infrared. *Journal of Geophysical Research* 88, 9723–9735.

Grenfell, T.C., 1991. Radiative transfer model for sea ice with vertical structure variations. *Journal of Geophysical Research* 96, 16991–17001.

Grenfell, T.C., Perovich, D.K., 1981. Radiation absorption coefficients of polycrystalline ice from 400–1400 nm. *Journal of Geophysical Research* 86 (C8), 7447–7450.

Haines, E.M., Buckley, R.G., Trodahl, H.J., 1997. Determination of the depth dependent scattering coefficient in sea ice. *Journal of Geophysical Research* 102 (C1), 1141–1151.

Hanesiak, J.M., Barber, D.G., De Abreu, R.A., Yackel, J.J., 2001. Local and regional albedo observations of Arctic first-year sea ice during melt ponding. *Journal of Geophysical Research* 106 (C1), 1005–1016.

Holland, M.M., Bitz, C.M., Hunke, E.C., Lipscomb, W.H., Schramm, J.L., 2006. Influence of the sea ice thickness distribution on polar climate in CCSM3. *Journal of Climate* 19 (11), 2398–2414.

Light, B., Maykut, G.A., Grenfell, T.C., 2003. Effects of temperature on the microstructure of first-year Arctic sea ice. *Journal of Geophysical Research* 108 (3051).

Lindsay, R.W., Zhang, J., 2005. The thinning of Arctic sea ice, 1988–2003: have we passed a tipping point? *Journal of Climate* 18 (22), 4879–4894.

Maffione, R.A., Voss, J.M., Mobley, C.D., 1998. Theory and measurements of the complete beam spread function in sea ice. *Limnology and Oceanography* 43, 34–43.

Maslanik, J.A., Fowler, C., Stroeve, J., Drobot, S., Zwally, J., Yi, D., Emery, W., 2007. A younger, thinner Arctic ice cover: increased potential for rapid, extensive sea-ice loss. *Geophysical Research Letters* 34 (L24501).

Maykut, G., Grenfell, T.C., 1975. The spectral distribution of light beneath first-year sea ice in the Arctic Ocean. *Limnology and Oceanography* 20 (4), 554–563.

Maykut, G.A., Light, B., 1995. Refractive index measurements in freezing sea ice and sodium chloride brines. *Applied Optics* 34, 950–961.

Parkinson, C.L., Cavalieri, D.J., Gloersen, P., Zwally, H.J., Comiso, J.C., 1999. Arctic sea ice extents, areas and trends, 1978–1996. *Journal of Geophysical Research* 104 (C9), 20837–20856.

Pegau, W.S., Zaneveld, J.R.V., 2000. Field measurements of in-ice radiance. *Cold Regions Science and Technology* 31, 33–46.

Perovich, D.K., 1996. *The Optical Properties of Sea Ice*. Monograph 96-1, US Army Corps of Engineers, Cold Regions Research & Engineering Laboratory.

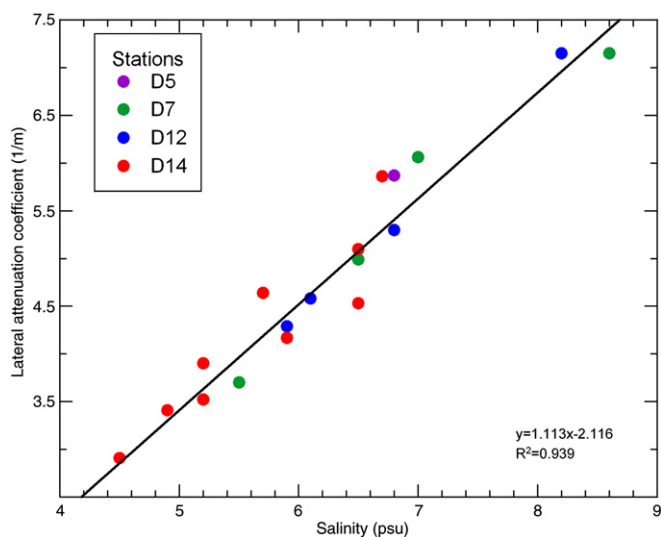


Fig. 8. Correlation of the attenuation coefficient of LPL with salinity in sea ice for the light of 490 nm. Data for all stations are used with the exception of D10 in which no salinity is measured. The attenuation coefficients are highly correlated to the salinity of sea ice. The correlation coefficients $R^2 = 0.939$.

- Perovich, D.K., Grenfell, T.C., 1981. Laboratory studies of the optical properties of young sea ice. *Journal of Glaciology* 27, 331–346.
- Perovich, D.K., Longacre, J., Barber, D.G., Maffione, R.A., Cota, G.F., Mobley, C.D., Gow, A.J., Onstott, R.G., Grenfell, T.C., Pegau, W.S., Landry, M., Roesler, C.S., 1998. Field observations of the electromagnetic properties of first-year sea ice. *Transactions on Geoscience and Remote Sensing* 36 (5), 1705–1715.
- Schoonmaker, J.S., Voss, K.J., Gilbert, G.D., 1989. Laboratory measurements of optical beams in young sea ice. *Limnology and Oceanography* 34 (S), 1606–1613.
- Trodahl, H.J., Buckley, R.G., Brown, S., 1987. Diffusive transport of light in sea ice. *Applied Optics* 26, 3005–3011.
- Trodahl, H.J., Buckley, R.G., Vignaux, M., 1989. Anisotropic light-radiance in and under sea ice. *Cold Regions Science and Technology* 16, 305.
- Tucker III, W.B., Weatherly, J.W., Eppler, D.T., Farmer, L.D., Bentley, D.L., 2001. Evidence for rapid thinning of sea ice in the western Arctic Ocean at the end of the 1980s. *Geophysical Research Letters* 28, 2851–2854.
- Voss, K.J., Schoonmaker, J.S., 1992. Temperature dependence of beam scattering in young sea ice. *Applied Optics* 31, 3388–3389.
- Voss, K.J., Honey, R.C., Gilbert, G.D., Buntzen, R.R., 1992. Measuring the point spread function of sea ice in situ. In *Proceedings of SPIE Ocean Optics XI*, vol. 1750, pp. 517–522.
- Zhao, J.-P., Barber, D., Li, T., Li, S.-J., Li, X., 2008. Radiation of lamp and optimized experiment using artificial light in the Arctic Ocean. *Chinese Journal of Polar Science* 19 (2), 249–260.